JACS
JOURNAL OF THE AMERICAN CHEMICAL SOCIETY

Article

pubs.acs.org/JACS

Multifunctional Two-Photon Active Silica-Coated Au@MnO Janus Particles for Selective Dual Functionalization and Imaging

Isabel Schick,[†] Steffen Lorenz,[‡] Dominik Gehrig,[§] Anna-Maria Schilmann,[†] Heiko Bauer,[†] Martin Panthöfer,[†] Karl Fischer,[∥] Dennis Strand,[‡] Frédéric Laquai,[§] and Wolfgang Tremel*[,†]

[†]Institut für Anorganische Chemie und Analytische Chemie, Johannes Gutenberg-Universität, Duesbergweg 10-14, 55128 Mainz, Germany

[‡]Medizinische Klinik, Universitätsmedizin der Johannes Gutenberg-Universität, Langenbeckstrasse 1, 55131 Mainz, Germany

[§]Max-Planck-Institut für Polymerforschung, Max-Planck-Forschungsgruppe für Organische Optoelektronik, Ackermannweg 10, 55128 Mainz, Germany

[∥]Institut für Physikalische Chemie, Johannes Gutenberg-Universität, Jakob-Welder-Weg 11, 55128 Mainz, Germany

Supporting Information

ABSTRACT: Monodisperse multifunctional and nontoxic Au@MnO Janus particles with different sizes and morphologies were prepared by a seed-mediated nucleation and growth technique with precise control over domain sizes, surface functionalization, and dye labeling. The metal oxide domain could be coated selectively with a thin silica layer, leaving the metal domain untouched. In particular, size and morphology of the individual (metal and metal oxide) domains could be controlled by adjustment of the synthetic parameters. The SiO_2 coating of the oxide domain allows biomolecule conjugation (e.g., antibodies, proteins) in a single step for converting the photoluminescent and superparamagnetic Janus nanoparticles into multifunctional efficient vehicles for theranostics. The Au@MnO@SiO_2 Janus particles were characterized using high-resolution transmission electron microscopy (HR-)TEM, powder X-ray diffraction (PXRD), optical (UV−vis) spectroscopy, confocal laser fluorescence scanning microscopy (CLSM), and dynamic light scattering (DLS). The functionalized nanoparticles were stable in buffer solution or serum, showing no indication of aggregation. Biocompatibility and potential biomedical applications of the Au@MnO@SiO_2 Janus particles were assayed by a cell viability analysis by coincubating the Au@MnO@SiO_2 Janus particles with Caki 1 and HeLa cells. Time-resolved fluorescence spectroscopy in combination with CLSM revealed the silica-coated Au@MnO@SiO_2 Janus particles to be highly two-photon active; no indication for an electronic interaction between the dye molecules incorporated in the silica shell surrounding the MnO domains and the attached Au domains was found; fluorescence quenching was observed when dye molecules were bound directly to the Au domains.

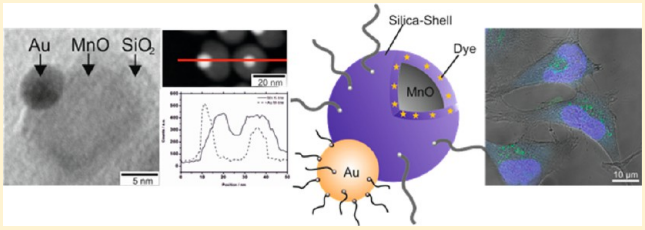

INTRODUCTION

The synthesis of complex colloids consisting of two or more inorganic or organic phases in the same nanoparticle offers a wealth of opportunities for applications.[1] Besides conventional hybrid materials such as core−shell,[2−5] alloy,[6−9] or bimetallic heterostructures,[10−13] a new generation of Janus-type particles with two regions of different chemical composition within the same particle has emerged during the past years. This combination of materials with distinctly different chemical and physical properties yields unique nanohybrids with multifunctional capabilities and tunable or even enhanced properties that might not be attainable otherwise.[14]

Janus particles have long been fascinating objects in the study of self-assembly, in the stabilization of emulsions, as dual-functionalized optical, electronic, and sensor devices.[15,16] Janus particles have been obtained originally from dendrimers[17,18] and block copolymer micelles,[19,20] but recently also from inorganic nanoparticles containing gold,[21−24] silver,[21,22,25,26] platinum,[27−29] alloy,[30,31] or 3d metals,[32−35] and oxide, metal and metal sulfide[36−45] components, or semiconductor NPs.[19,20] Potential applications of Janus particles are determined by the combination of materials building up the hemispheres. For example, particles with oppositely charged hemispheres have a large dipole moment, which allows remote positioning in an electric field.[46,47] When loaded with distinct drugs or dyes, the particles have potential biomedical applications.[48−50] Moreover, catalytically or electrochemically active metal components (e.g., Au, Pt, or Ni)[51,52] in combination with magnetic materials have received attention, because the noble metals can be recovered magnetically after use, while still retaining the desired catalytic properties. In addition, wavelength-tunable photovoltaic and photocatalytic materials with efficient charge separation

Received: October 22, 2013
Published: January 26, 2014

 © 2014 American Chemical Society dx.doi.org/10.1021/ja410787u | J. Am. Chem. Soc. 2014, 136, 2473−2483

capabilities may be achieved with heterostructures incorporating nanocrystals with size-tunable properties.[53,54]

Heteroparticles with tunable composition and morphology exhibit multiple functionalities that have been proven useful for synchronous biolabeling, separation, detection, and multimodal imaging in biomedicine.[48−50,55] In particular, Au@semiconductor hybrid nanoparticles have become an active frontier of research.[56,57] Of the various groups of nanomaterials, Au nanoparticles show an unusually high polarizability of optical frequencies arising from the excitation of localized surface plasmon resonances.[58,59] Au nanoparticles generate an intense optical signal, they are durable and apt to bind molecules of interest in a controlled fashion without photobleaching, a major drawback of common fluorescent dyes.[60] Furthermore, their strong X-ray absorption coefficient together with the easiness of thiol functionalization makes them nearly ideal contrast agents for computer tomography.[61] Additionally, gold nanoparticles have promising therapeutic properties as hyperthermal agents because the local temperature around gold nanoparticles can be increased by laser illumination through the tunable surface plasmon bands in the near-infrared region (NIR).[62−65]

Moreover, gold rods showed strong two-photon activity in cellular imaging.[66−74] Multiphoton microscopy possesses some advantages over conventional confocal microscopy, such as reduced fluorescence background because of the relatively low two-photon cross-section of most biomolecules responsible for autofluorescence, reduction of photobleaching by selective excitation of the focal volume, and improved depth penetration in scattering samples by using excitation light within the optical transmission window of biological tissues (near-infrared (NIR) spectral range, 700−1000 nm).[68]

Magnetic nanoparticles, on the other hand, constitute a class of nanomaterials that has attracted much research effort for biomedical applications.[75−79] Magnetic nanoparticles have been studied for protein separation,[80,81] as tags for the *in vitro* detection of biomarkers,[82] and as analytical probes for cell tracking,[83] magnetic resonance imaging,[84,85] and multimodal imaging.[22,86−90] Furthermore, they are the basis for magnetic nanoparticle-based therapeutics such as hyperthermia, drug delivery, and gene delivery.[48−50]

Unlike iron oxide (Fe_3O_4) nanoparticles, which are mostly used as T_2 contrast probes by causing hypointensities in magnetic resonance imaging (MRI),[90,91] superparamagnetic manganese oxide (MnO) nanoparticles induce hyperintensities on T_1-weighted MRI maps and, therefore, can be diagnostically more informative.[92]

One of the drawbacks of Fe_3O_4 and MnO are the toxic effects of the bare, uncoated nanoparticles, whereas ligand-coated nanoparticles have shown lower toxic effects, depending on the constitution of the protection shell.[93−95] Therefore, the formation of a silica coating around the metal oxide component offers advantages such as chemical and physical protection from the surrounding environment, stability in aqueous media, and a platform for further modification.[4,96] The well-developed surface chemistry for silica provides an opportunity to specifically tune the particle properties for later applications, but a continuous silica shell around the Janus particles would re-establish the lack of surface addressability of a single component particle.[97]

Here, we present a method for the synthesis of a multifunctional Au@MnO Janus particle, where only the metal oxide component has been coated with a thin silica layer. This is based on the reduced wetting of the chemically different surfaces, which leaves the noble metal component untouched and available for specific surface functionalization that allows a facile conjugation of biomolecules. Au@MnO@SiO_2 Janus particles are useful not only for simultaneous magnetic and optical detection but also for medical targeting. They are highly biocompatible and two-photon active and thus are alternatives to current nanoparticle platforms for biomedical/bioimaging applications.

EXPERIMENTAL SECTION

Materials. Tetrachloroauric(III) acid hydrate (51% Au, $HAuCl_4{\cdot}(H_2O)_x$) and 2-methoxy-(polyethyleneoxy)-propyltrimethoxysilane (PEG-silane, n = 9−12) (90%) were purchased from ABCR. Tetralin (1,2,3,4-Tetrahydro-naphthalene) (anhydrous, 99%), borane *tert*-butylamine complex (TBAB) (97%), 1-octadecanethiol (ODT) (98%), manganese(II)-chloride tetrahydrate ($MnCl_2{\cdot}4H_2O$) (Reagent Plus, >99%), sodium hydroxide (99%), 1-octadecene (90%), Igepal CO-520, ammonium hydroxide (25%, aqueous solution), 3-aminopropyl-triethoxysilane (APS) (>99%), tetraethoxysilane (TEOS) (>99%), and fluorescein 5(6)-isothiocyanate (FITC) were purchased from Aldrich. Oleylamine (80−90%), oleic acid (Reagent grade), toluene, methanol, hexane, cyclohexane, and acetone were purchased from Fisher Scientific. All chemicals were used without further purification.

Synthesis of Au Nanoparticles and Ligand Exchange. Monodisperse gold nanoparticles were prepared by reduction of tetrachloroauric acid in tetralin as reported by Sun et al.[98] Briefly, a precursor solution containing 0.3 mmol $HAuCl_4{\cdot}(H_2O)_x$, 10 mL oleylamine, and 10 mL tetralin was prepared at room temperature. TBAB (0.5 mmol) was dispersed in 1 mL tetralin and 1 mL oleylamine by sonification and added quickly to the precursor solution. At room temperature, the reaction yields monodisperse Au nanoparticles with a diameter of 4 nm, whereas lowering the temperature to 10 °C leads to 8 nm particles; at 40 °C 2 nm particles are produced. The reaction solution was stirred for 1 h before precipitating the particles using methanol and collecting them by centrifugation. The particles were washed using hexane/ethanol. The Au nanoparticles are soluble in nonpolar solvents in general, for example, in hexane, chloroform, and toluene.

The ligand exchange to 1-octadecanethiol was performed by addition of a solution of oleylamine-functionalized Au-NP to 10 mL toluene containing 3 mmol ODT under argon atmosphere. The solution was stirred at room temperature overnight. The particles were precipitated, collected by centrifugation, and washed using hexane/ethanol.

Synthesis of Au@MnO Heterodimers. Heteroepitaxial growth of manganese oxide on ODT-functionalized gold particles was used for the preparation of monodisperse Au@MnO heterodimers with tunable size of the MnO domains. For 4@25 nm-heterodimers, 0.4 mmol manganese(II) oleate[99] was mixed with 20 mL 1-octadecene containing 6 mmol oleic acid and 6 mmol oleylamine at 80 °C under argon atmosphere. Ten milligrams ODT-functionalized Au nanoparticles in 1 mL 1-octadecene were added to the mixture which was degassed at 80 °C for 1 h and slowly heated up to 315 °C (heating rate: 2 °C/min). The reaction mixture was held at reflux for 90 min before cooling down to room temperature by removing the heating mantle. The particles were washed by repeated precipitation with acetone, centrifugation, and dissolution in hexane.

Scheme 1. Seed-Mediated Synthesis of Au@MnO Heterodimers, Subsequent Encapsulation with Silica and Functionalization of the SiO_2-Shell As Well As the Au Domain

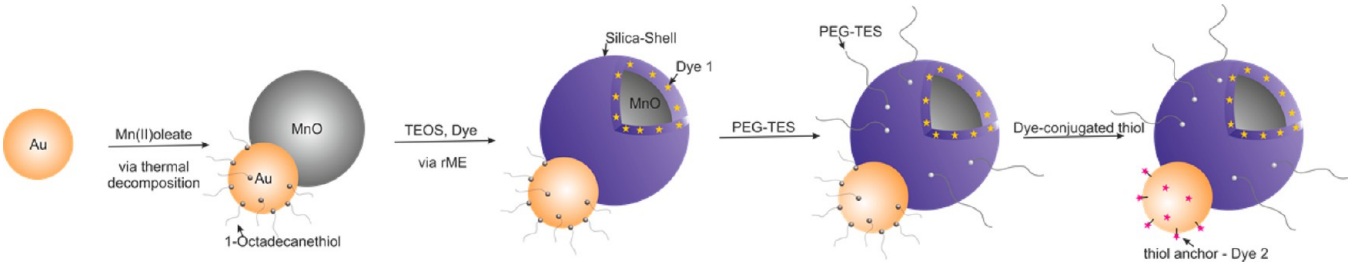

Silica Encapsulation of the MnO Domain of Au@MnO Heterodimers. The MnO domains of hydrophobic Au@MnO heterodimers were encapsulated with SiO_2 using the reverse microemulsion technique as reported previously.[96] Briefly, 2.0 g Igepal CO-520 was dissolved in 35 mL cyclohexane and degassed for 15 min using a gentle stream of argon. Roughly 10 mg of nanoparticles in 1 mL cyclohexane were added, and the degassing procedure was continued for another 15 min. Aqueous NH_4OH (200 μL) was added dropwise to induce micelle formation. TEOS (112 μL) (and FITC or APS-Atto495-conjugate[96] in DMF for dye-labeled nanoparticles) were added after 5 min, and the reaction mixture was stirred under argon atmosphere overnight. Further functionalization of the shell was achieved by addition of PEG-silane (130 μL), which led to complete precipitation of the Au@MnO@SiO_2 nanoparticles within 2 h. The nanoparticles were collected by centrifugation and washed several times by dissolution in acetone and precipitation with hexane.

To increase the number of amino groups on the surface of the silica shell the nanoparticles were dissolved in 20 mL of acetone. The amino groups were inserted by addition of APS (150 μL, 0.64 mmol) and aqueous NH_4OH (150 μL). The mixture was stirred under argon atmosphere for another 4 h. The product particles were precipitated using hexane, collected by centrifugation (5000 rpm, 5 min), and dissolved in acetone. The nanoparticles were washed several times using hexane/acetone. The obtained particles were easily soluble in acetone, ethanol, DMF/DMSO, and various aqueous media

Nanoparticle Characterization. The particles were characterized by means of (high resolution) transmission electron microscopy ((HR-)TEM), Fourier transformed infrared spectroscopy (FT-IR), atomic absorption spectroscopy (AAS), UV−vis, and fluorescence spectroscopy. HR-TEM images were recorded using a FEI Tecnai F30 S-TWIN instrument with a 300 kV field emission gun, low-resolution TEM images using a Philips EM420 microscope with an acceleration voltage of 120 kV. Samples for HR-TEM were prepared by dropping a dilute solution of nanoparticles in the appropriate solvent (hexane, acetone, water) onto a carbon-coated copper grid (Plano, Wetzlar; Germany). FT-IR spectra were measured on a Bruker Tensor 27 spectrometer. The concentration of aqueous nanoparticles solutions was determined by AAS (Perkin-Elmer 5100 ZL): Aliquots were treated with conc. HNO_3 at 90 °C for 10 min followed by adjusting the pH value using NH_4OH. UV−vis spectra were collected by a Varian Cary 5000 UV−vis/NIR spectrometer.

Dynamic light scattering measurements (DLS) were performed using a Uniphase He/Ne Laser (λ = 632.8 nm, 22 mW), a ALV-SP125 Goniometer, a ALV/High QE APD-Avalanche photodiode with fiber optical detection, a ALV 5000/E/PCi-correlator and a Lauda RC-6 thermostat unit. Angular dependent measurements were carried out in the range $30° \leq \theta \leq 150°$. For data evaluation experimental intensity correlation functions were transformed into amplitude correlation functions applying the Siegert relation extended to include negative values after baseline subtraction by calculation $g_1(t)$ = SIGN($G2(t)$)· SQRT(ABS(($G2(t) - A$)/A).

$g_1(t)$ was evaluated by fitting a biexponential function $g_1(t) = a\cdot\exp(-t/b) + c\cdot\exp(-t/d)$ to take polydispersity into account. Average apparent diffusion coefficients, D_{app}, were determined according to $q^2\cdot D_{app} = (a\cdot b^{-1} + c\cdot d^{-1})/(a+c)$. $D_{app}(q = 0)$ was extrapolated from that data. Hydrodynamic radii were then extracted from the Stokes−Einstein equation. For DLS measurements sample concentrations were in the range from $5 < c < 100$ mg/L. Low salt concentrations (10^{-5} M NaBr) were added in the case of silica-coated particles in water in order to prevent fast/slow mode splitting in DLS due to Coulombic interaction. All samples were filtered into dust free cylindrical scattering cells (Hellma, Suprasil, 2 cm diameter) using syringe filters (Millipore LCR 450 nm *n*-heptane solutions, PALL GHP 200 nm water solutions). Filtration losses were checked to be well below 10%.

Two-photon analysis was carried out using a Zeiss LSM 710 NLO microscope equipped with Non Descanned Detectors (NDDs) and a Coherent Chameleon Ultra II Ti:Sapphire Laser. For image acquisition a LD C-Apochromat 40×/1.1 W Korr M27 objective was used, and the samples were excited at 970 nm. Twelve percent laser power 30 mW was used for imaging, while 10% laser power was used for bleaching experiments (for 110 s) with 5% laser power as reference (see Figure S4 in Supporting Information [SI]). The emitted fluorescence was passed through 455−500, 500−550, and 656−610 band-pass filters to NDDs. All data were acquired and processed using the Zen 2009 software (Carl Zeiss, Germany).

Time-Resolved Fluorescence Spectroscopy. Transient emission spectra on a picosecond time scale were taken with a Streak Camera System (Hamamatsu C4742). The excitation wavelength was 400 nm provided by the frequency-doubled output of a Coherent MIRA Ti:Sapphire laser system.

Cell Culture and Cytotoxicity Assay. Human renal cell carcinoma cell line (Caki-1) and human cervical cell carcinoma cell line (HeLa) were kindly provided by Prof. P. Langguth (Institute for pharmacy and biochemistry, Johannes Gutenberg-University, Mainz). McCoys 5A medium was used as culture medium and modified by addition of 10% fetal bovine serum (FBS, Sigma-Aldrich), 1% penicillin−streptomycin (PEST, 1000 U/mL penicillin and 10 mg/mL streptomycin, Sigma-Aldrich), 2 mM L-glutamine (Sigma-Aldrich, Germany), Mycokill (PAA, Germany), and MEM nonessential amino acids (Sigma-Aldrich, Germany). Cells were routinely grown in

dx.doi.org/10.1021/ja410787u | J. Am. Chem. Soc. 2014, 136, 2473−2483

25 cm^2 sterile cell culture flasks at 37 °C, 95% relative humidity, and 5% CO_2 until confluence was reached. The cytotoxicity assay was performed according to the supplier in 96,well cell plates used under standard conditions. The density was 15,000 cells/well. For background subtraction 6 wells were filled only with media and H_2O. After 24 h of cell growth, different concentrations of polymer-functionalized or silica-coated nanoparticles in McCoys 5A were added, and the incubation time was set to 24 h. The medium was then replaced by 100 μL of a cell counting kit solution (5.4 mL culture medium was mixed with 600 μL CCK8, Sigma-Aldrich) and incubation at 37 °C, 95% relative humidity, and 5% CO_2 was continued for another 3 h. The absorption of formazan formed due to cellular activity was measured at 450 nm. All results were normalized to wells that contained media instead of cells, after background subtraction.

RESULTS AND DISCUSSION

Particle Synthesis and Silica Coating. The synthetic route for the preparation of the multifunctional silica-coated and thiol-functionalized Au@MnO heterodimers is illustrated in Scheme 1. The oleylamine-capped Au nanoparticles were synthesized following a procedure described by Sun et al., in which the size of the particles can be varied between 2 and 8 nm by changing the reaction temperature.[98] In a subsequent step, the hydrophobic, oleate-capped MnO domains were synthesized based on the formation of monodisperse MnO nanoparticles.[99] The MnO domains were nucleated heterogeneously on the Au seeds by the decomposition of a manganese oleate precursor. The formation of heteronanoparticles can be achieved by suppressing homogeneous nucleation and, simultaneously, by promoting heterogeneous nucleation.[100] Homogeneous nucleation can be suppressed by maintaining the precursor concentration below the critical supersaturation value. This was obtained by precise control of the precursor ratio, number of seed particles, and heating profile. In a subsequent step, the MnO domains of the Au@MnO heterodimers were encapsulated with SiO_2 embedding a dye (e.g., FITC, RITC, Atto495), by using the reverse microemulsion technique reported by Schladt et al.[96] Further surface functionalization of the silica shell is possible by adding a PEG-silane conjugate (PEG-TES) to promote the water solubility and biocompatibility. In addition, 3-aminopropyltriethoxysilane (APS) can be used to introduce amino groups, allowing further conjugation to biomolecules. The silica shell forms only around the metal oxide domains and leaves the gold surfaces untouched, so that an additional functionalization, by the addition of thiols, remains possible.

Nanoparticle Characterization. The synthesis of gold nanoparticles as well as Au@MnO heterodimers was monitored by transmission electron microscopy. Figure 1 shows oleylamine-capped Au nanoparticles prior to thiol functionalization. The particles are highly uniform in size and shape, with an average diameter of 4 nm ($\sigma \leq 5\%$). This gives reason to the high degree of order and the self-assembly to two-dimensional (2D) (Figure 1a) and three-dimensional (3D) (Figure 1b) superlattices. The use of these gold nanoparticles as seeds for the synthesis of Au@MnO heteronanoparticles leads to the formation of "flower-like" particles, due to multiple nucleation of MnO.[24] The resulting "flower-like" Au@MnO heteronanoparticles are shown in Figure 2a. The formation of heterodimers is promoted by functionalizing the gold nanoparticles with a thiol prior to the thermal decomposition of manganese oleate. Due to the higher binding affinity of the thiols to gold, the surface protection of gold nanoparticles is stronger compared to amines, and multiple nucleation is suppressed.

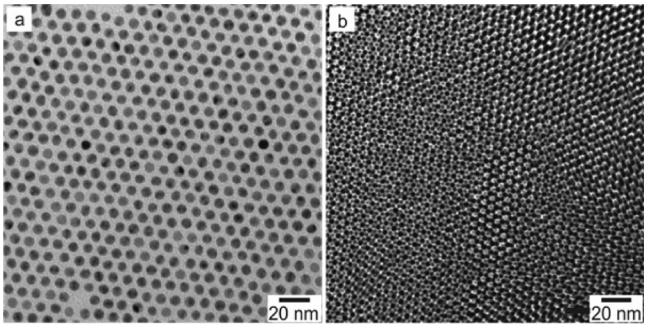

Figure 1. HR-TEM bright field images of 4 nm Au nanoparticles: (a) 2D superlattice, (b) 3D-superlattice.

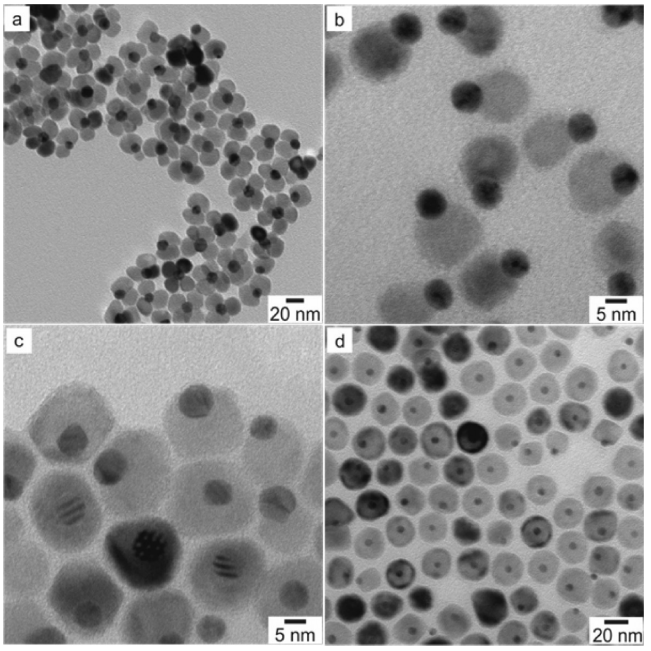

Figure 2. TEM bright field images of Au@MnO heteronanoparticles (a) "flowerlike" nanoparticles; heterodimer-nanoparticles with tunable sizes of the Au and MnO domain: (b) 7@15 nm, (c) 7@20 nm, and (d) 4@25 nm.

For Au nanoparticles of a given size, the diameter of the MnO domains can be varied between 10 and 30 nm, depending on the amounts of the manganese oleate precursor and the oleylamine and oleic acid ligands. To synthesize Janus particles with different MnO domain sizes, the ratio of manganese oleate to gold seeds was varied between 0.2 and 0.4 mmol manganese oleate per 10 mg Au nanoparticles. The resulting heterodimers were highly monodisperse ($\sigma \leq 10\%$). Representative TEM images of particles with various domain sizes are shown in Figure 2. Independent of the ratio of the gold seeds to the manganese oleate, no isolated MnO particles were observed. The presence of pure Au nanoparticles could be suppressed by the precise control of the surfactants. Particles with a larger MnO domain ($\geq$20 nm) order in a hexagonal fashion with respect to the MnO domains, while particles with smaller MnO domains lie flat on one side, showing the morphology of heterodimers. The self-assembly of heterodimers with small Au

dx.doi.org/10.1021/ja410787u | J. Am. Chem. Soc. 2014, 136, 2473−2483

domains is determined by the spherical shape of the MnO domains. Due to their low polydispersity (≤10%) the heterodimers form well-ordered hexagonal close-packed layers. Upon increasing the size ratio (r_{Au}/r_{MnO}) a tendency to a side-on arrangement was observed.

TEM-EDX line scans were performed to study the particle morphology (Figure 3). The spatially resolved element mapping of manganese, gold, and oxygen, as well as TEM tomography (see Figure S2 in SI) shows the heteronanoparticles to be Janus-type dimers.

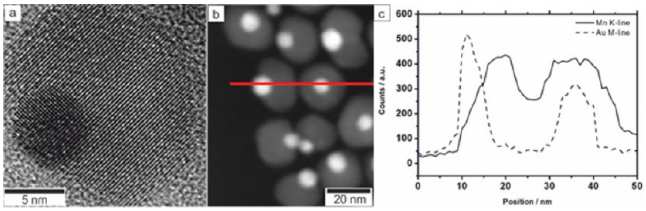

Figure 3. (a) HR-TEM bright field image, (b) HAADF-STEM image, and (c) Au and Mn elemental profiles of Au@MnO Janus particles.

The heteroepitaxial growth of the MnO domains on the gold seeds changes the local dielectric function of their surrounding medium, and, therefore, the position of the maximum of the plasmon absorption band. Figure 4 shows the shift of the

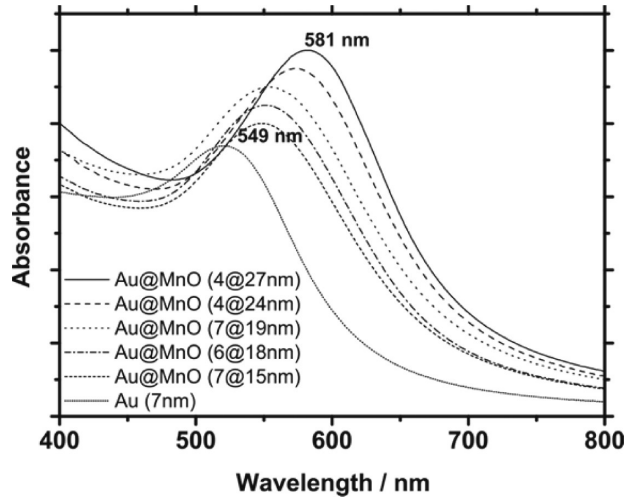

Figure 4. UV−vis spectra of Au@MnO heterodimers as a function of the domain sizes in comparison to pristine Au nanoparticles.

absorption maximum of the gold particles by about 30−70 nm compared to the absorption of pure Au nanoparticles (~510−520 nm, depending on parameters like particle morphology, size, solvent according to Miés theory),[101,102] and may be estimated quantitatively with the aid of literature values for the optical constants for Au nanoparticles. The red shift is caused by the conjugation to an electron-deficient material (MnO), and the dependence of the wavelength on the density of electrons, effective electron mass, as well as shape and size of charge distribution.[103] The experimental results confirm the assumption that the Au@MnO Janus particles are both magnetically (i.e., superparamagnetic, see Figure S5 in SI) and two-photon active, making them ideal candidates for multimodal biomedical imaging.

Selective Functionalization and Solution Stability. We investigated the individual addressability of both gold and silica surfaces. The distinct wetting of the Au@MnO heterodimers was used to encapsulate the MnO domain within the silica shell, in a manner the same as that reported for the silica coating of MnO nanoparticles.[96] Due to the selective addressability of the dimer domains, the gold component remained untouched by silica; no multiple nanoparticles were found within a silica shell. Figure 5 shows Au@MnO@SiO_2

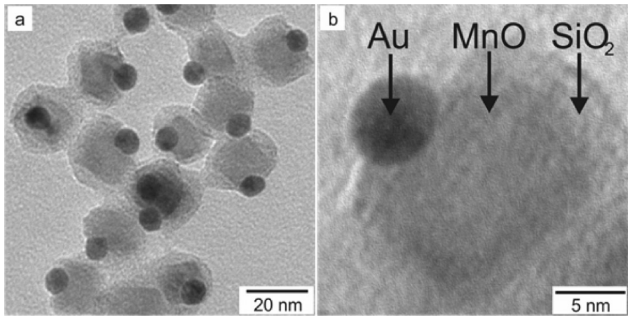

Figure 5. (a) Overview TEM bright field image of Au@MnO@SiO_2 nanoparticles, (b) TEM micrograph of a single Au@MnO@SiO_2 particle.

nanoparticles after the functionalization was complete. The thickness of the silica shell (~3 nm) is consistent with the results reported for pure MnO particles. The nanoparticles appear uniform and well separated, even though, they are functionalized orthogonally.

The phase composition of the as-prepared Au@MnO Janus particles was investigated by powder X-ray diffraction. Figure S1 (SI) displays typical powder XRD patterns of Au@MnO Janus particles, with domain sizes of 7 nm@14 nm (see Figure S1b in SI) and 4 nm@25 nm (see Figure S1c in SI), as well as Au@MnO@SiO_2 (10 nm@19 nm, 5 nm SiO_2 shell). The positions and relative intensities of all reflections are in good accordance with expected patterns for *fcc*-type Au and rock-salt-type MnO. Crystallite sizes determined from the reflection profiles are in good agreement with the particle and crystallite sizes observed in the TEM measurements. Small Au (~4 nm) domains are mostly single crystalline. Bigger domains (~7 nm) tend to be twins or polycrystals (see Table S1 in SI). Due to the crystallite sizes the profile of the Au reflections is broader than that of the MnO reflections. In comparison to the uncoated particles, the XRD pattern of the coated particles exhibits a very broad, structureless diffraction maximum centered at approximately $Q = 1.33/A$, which is due to the amorphous silica coating. (Figure S1 in SI)

The formation of the silica shell was monitored by FT-IR spectroscopy. Figure 6 displays FT-IR-spectra of Au@MnO nanoparticles prior to, as well as after the silica encapsulation. The spectrum of oleylamine- and oleic acid-capped Au@MnO nanoparticles (dashed line, top) displays characteristic vibrational bands at 1555 and 1410 cm^{-1}, assigned to the asymmetric and symmetric stretching modes of the carboxylate groups of oleic acid, and the strong absorption bands at 2850, 2922, and 2958 cm^{-1}, assigned to the symmetric and asymmetric stretching modes of the CH_2- and CH_3-groups.[99] In the spectrum of the Au@MnO@SiO_2 particles, the bands of the carboxylate groups have vanished almost completely. A broad and strong band system in the region between 1200 and

dx.doi.org/10.1021/ja410787u | J. Am. Chem. Soc. 2014, 136, 2473−2483

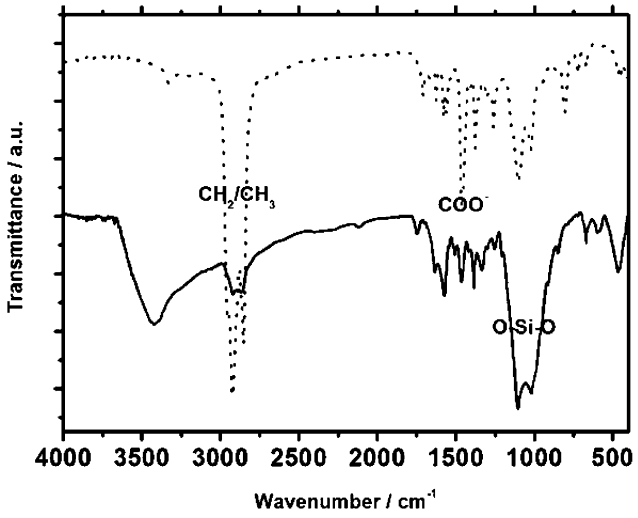

Figure 6. FT-IR-spectra of Au@MnO (dashed) and Au@MnO@SiO_2 nanoparticles (solid). Due to the encapsulation with silica, the stretching modes of the carboxylic groups disappear, whereas strong O−Si−O modes emerge.

1000 cm^{-1} appears instead, which is assigned to the O−Si−O stretching modes. The stretching vibrations due to CH_2- and CH_3-groups remain, although less pronounced, due to the conjugation of PEG-chains to the surface of the silica shell as well as the ligands of the Au domains.[97]

Selective functionalization of the Au domain was achieved by incubating an aqueous solution of Au@MnO@SiO_2 nanoparticles with thiol modified 24-mers customized oligonucleotide. The latter was tagged with TexasRed.[104] Excess reagents were removed by centrifugation.

The silica encapsulated particles Au@MnO@SiO_2 as well as the precursor particles Au@MnO were characterized by dynamic light scattering (DLS, Figure 7). As can be taken from the amplitude autocorrelation functions fits (Figure 7a) and the constancy of the apparent diffusion coefficients as a function of scattering angle (Figure 7b), both samples are highly monodisperse (from cumulant fits: $\mu_2 < 0.05$ for Au@MnO and Au@MnO@SiO_2 at $\theta = 90°$, ACFs not shown), with sizes of R_h(Au@MnO) = 15.7 nm ±0.2 nm and R_h(Au@MnO@SiO_2) = 21.5 nm ±0.1 nm. The increase of the hydrodynamic radius of about 6 nm is in good accordance with the thickness of the SiO_2 shell detected by TEM and the expected contribution of the hydration shell in solution. The inset of Figure 7a shows a digital photograph of the different nanoparticle solutions in water and different concentrations of human blood serum, respectively, directly after incubation up to 5 days at 22 °C.

Two-Photon Activity. The functionalized nanoparticles were analyzed under an epifluorescent microscope at different emission wavelengths to visualize the silica-coated MnO domains (green fluorescence) and the Texas Red-tagged Au domains (red fluorescence). The colocalization of the green/red fluorescence signals in Figure 8 supports the idea that the Janus particles could not only be efficient as cargo-specific carriers, but also be two-photon active, and, so, simultaneously be used as functional probes for multimodal targeted delivery and imaging. The colocalization was not as distinct as expected due to the quenching of the dye directly bound to the gold nanoparticles.

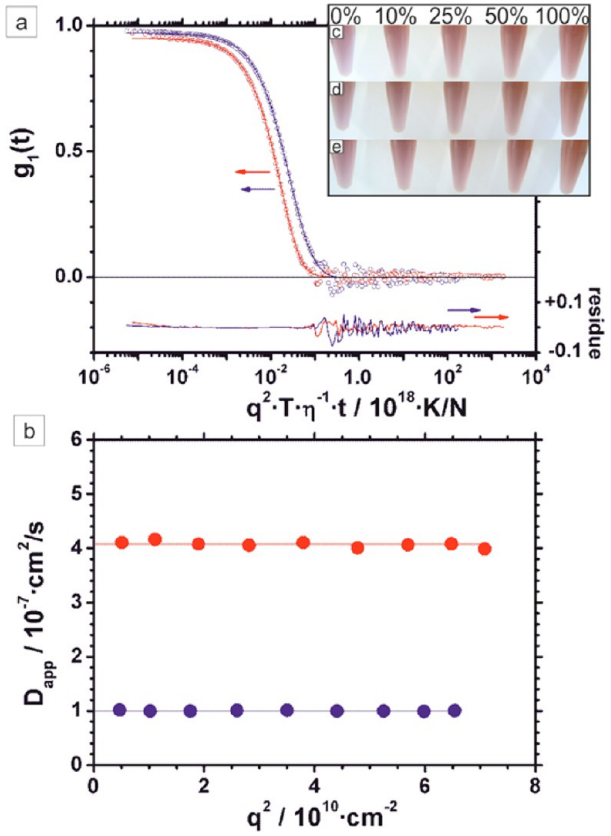

Figure 7. Dynamic light scattering results of (●, red) Au@MnO dispersed in *n*-heptane and (●, blue) Au@MnO@SiO_2 dispersed in water (λ = 632.8 nm, T = 293 K, viscosity η: 0.41 cP *n*-heptane, 1.005 cP water): (a) universally scaled and normalized field autocorrelation functions measured at scattering angle 30° together with biexponential fitting function lines and corresponding residues; (b) apparent diffusion coefficients as a function of scattering vector q^2 in the range of scattering angle $30° \leq \theta \leq 150°$. (Inset) stability of particle solutions in water and increasing amount of human blood serum (10% to 100% from left to right): (c) directly after incubation, (d) after 24 h, and (e) after 5 days.

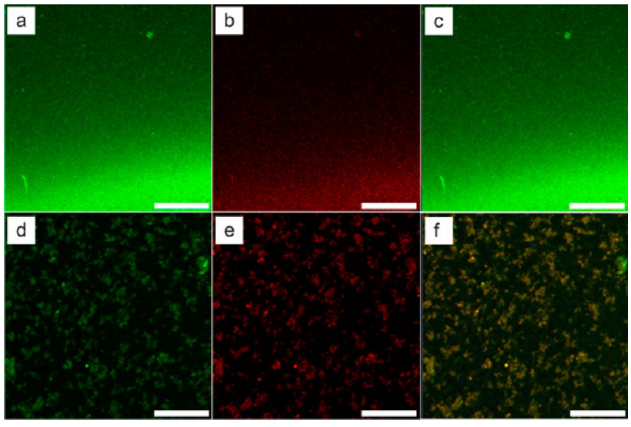

Figure 8. Fluorescence images of TexasRed−Au@MnO@SiO_2−Atto495 (a−c) and Au@MnO@SiO_2−Atto495 (d−f). From left to right: green channel, red channel, and overlay images. Scale: 20 μm.

In addition, strong two-photon activity was observed using an excitation wavelength of 970 nm, whereas an emission on red, green, and blue channels was measured (Figure 9). Due to fluorescence resonance energy transfer from the dye incorpo-

dx.doi.org/10.1021/ja410787u | J. Am. Chem. Soc. 2014, 136, 2473−2483

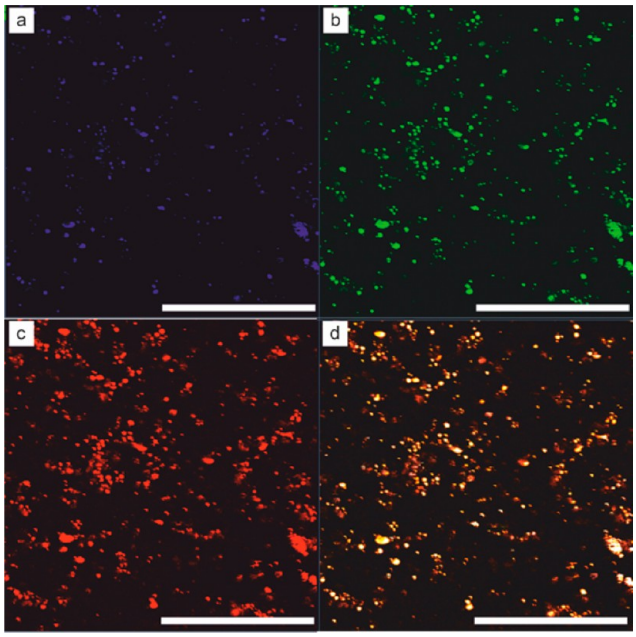

Figure 9. Two-photon fluorescence of Texas Red–Au@MnO@SiO_2–Atto495: (a), (b), and (c) fluorescence images showing emission in the blue, green, and red region, (d) overlay image. Excitation laser wavelength: 970 nm, Scale: 100 μm.

rated in the silica shell (Atto495) to the gold particles red fluorescence could be detected without any red dye. Therefore the particles may be used for optical detection in two different wavelength regions using only a single dye. But even without any dye, the particles show two-photon activity (Figure S6 in SI), which clearly shows the origin of the two-photon activity is the gold domain of the Janus particle and the activity superimposes with the two-photon activity of the encapsulated dye.

Excited State Dynamics. The fluorescence spectra and decay dynamics of the dye Atto495, of nanoparticles incorporating Atto495 and of pristine Au nanoparticles were systematically investigated by time-resolved photoluminescence spectroscopy (TR-PL). Aqueous solutions of the nanoparticles were excited by a femtosecond laser pulse at 400 nm and the subsequent emission was detected by a Streak Camera setup.

Pristine Atto495 showed single-exponential fluorescence dynamics (see Figure 10) with an inverse decay rate of 1.04 ns. The emission of Au nanoparticles did not decay exponentially, but could be described by a stretched exponential fitting function indicating a distribution of decay rates. A decay lifetime of 72 ps and a stretching exponent of 0.55 was obtained from the stretched exponential fit to the data. Attaching Atto495 to the surface of a SiO_2-coated MnO nanoparticle changed the excited state dynamics of the dye from a single-exponential to a biexponential decay. Fixing the longer decay component to the value found for pristine Atto495 resulted in a value for the shorter-lived decay component of 134 ps. The emission dynamics observed for the Au@MnO@SiO_2–Atto495 Janus particles could be described by a simple superposition of the dynamics observed for the pristine Au nanoparticles and the MnO@SiO_2–Atto495 nanoparticles. In fact, fixing the decay constants to the values obtained for the latter two yielded a fit that accurately described the emission dynamics of the Janus particles. Consequently, there is no indication for an electronic interaction between the dye molecules (Atto495) attached to the MnO@SiO_2 nanoparticles and the Au moiety within the same Janus particle.

Table 1. Inverse Decay Rates τ_1 and τ_2 Obtained from Fitting the Fluorescence Dynamics to a Single-Exponential (Atto495), a Stretched-Exponential (Au-NP), a Bi-exponential (MnO@SiO_2–Atto495) and a Combination of a Bi-Exponential and a Stretched-Exponential (Au@MnO@SiO_2–Atto495)[a]

Sample	τ_1 / ps	τ_2 / ps	β / s
Atto495	1040	---	---
Au-NP	72	-	0.55
MnO@SiO_2-Atto495	134	1040 (fixed)	-
Au@MnO@SiO_2-Atto495	134 (fixed) 72 (fixed)	1040 (fixed)	0.55 (fixed)

[a]Note that the dynamics in the latter is well-described by the dynamics observed for the individual components of the Janus particle.

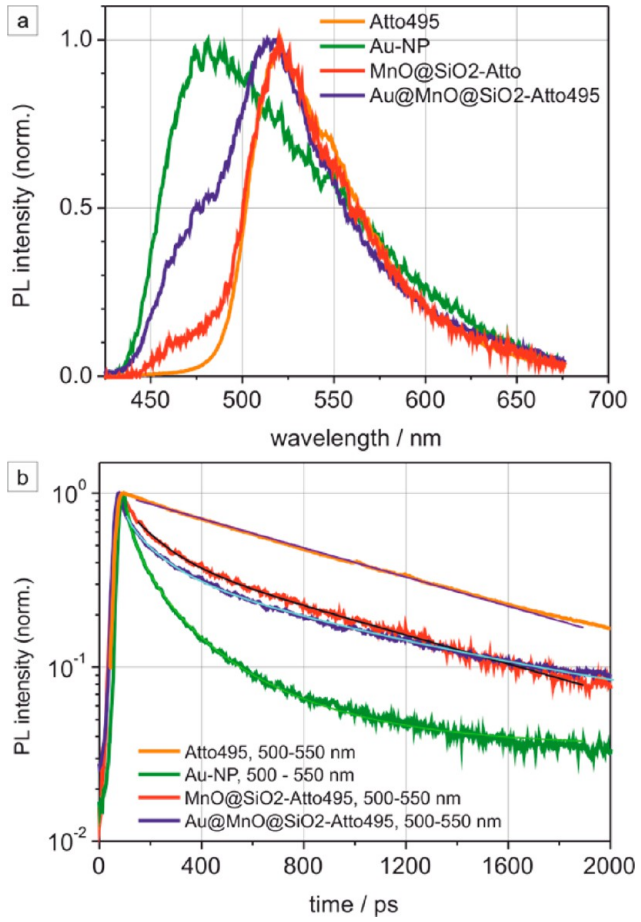

Figure 10. (a) Time-integrated emission spectra of pure Atto495 (orange), Au nanoparticles (green), MnO@SiO_2–Atto495 nanoparticles (red) and Au@MnO@SiO_2–Atto495 nanoparticles (blue). The samples were excited at 400 nm by a 100 fs laser pulse. (b) Fluorescence dynamics monitored at the emission peak wavelengths and fits according to the functions displayed in Table 1-.

dx.doi.org/10.1021/ja410787u | J. Am. Chem. Soc. 2014, 136, 2473–2483

Biocompatibility of the Particles. A potential biomedical use of silica coated Au@MnO Janus particles is targeted drug delivery using immunostimulatory oligonucleotides.[48,96,105,106] Therefore, the cytotoxic behavior of the Au@MnO@SiO_2 Janus particles was studied for human renal carcinoma cells (Caki) and human cervical carcinoma cells (HeLa).

Biocompatibility and potential biomedical applications of the Au@MnO@SiO_2 Janus particles were assayed by a cell viability analysis by coincubating the Au@MnO@SiO_2 Janus particles (8@16 nm Au@MnO, SiO_2 shell approximately 4 nm) with Caki 1 cells. A cell viability assay (for 24 h, 37 °C) revealed the Au@MnO@SiO_2 Janus particles to be non-cytotoxic, i.e. that in concentrations of 25, 50, and 100 μg/mL the percentage of cell survival was of 99.8 ± 5.0, 96.1 ± 4.8, and 94.4 ± 4.7%, respectively (Figure 11).

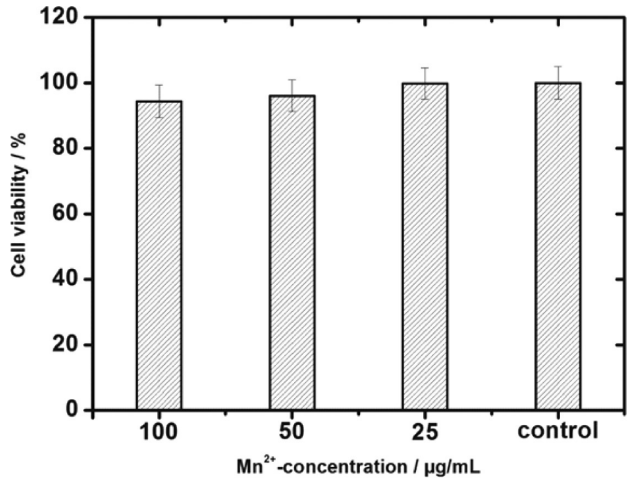

Figure 11. Vitality assay of Caki 1 cells incubated with Au@MnO@SiO_2 nanoparticles. The concentration of the nanoparticles is referred to the concentration of Mn^{2+} as measured by AAS.

Furthermore, we carried out cell imaging using confocal laser scanning microscopy. The instrumental background was set up so that cell self-fluorescence would not interfere with our measurements. Thus, we coincubated the Au@MnO@SiO_2 Janus particles (100 μg/mL) with HeLa cells for 24 h at 37 °C (Figure 12a and b). A significant cellular uptake was measured and confirmed by confocal *z*-stack images (see Figure S7 in SI). Panels c and d of Figure 12 show representative images of two-photon imaging (λ_{ex} = 970 nm, 30 mW), where the Au@MnO@SiO_2 Janus particles display a green luminescence (λ_{em} = 535 nm). No significant autofluorescence was observed under similar experimental conditions or under even higher excitation laser power.

The fluorescence from the Au nanoparticles may originate from radiative recombination of sp-band electrons and d-band holes, which could be enhanced by 4–6 orders of magnitude due to the surface plasmons of nanocrystals or rough metal surfaces. Previously, Au nanorods have shown strong two-photon fluorescence for cellular imaging.[66−74]

■ CONCLUSIONS

We demonstrated a facile synthetic method to fabricate water-stable and dispersible, highly biocompatible, and photoluminescent Au@MnO Janus particles by a seed-mediated nucleation and growth technique with precise control over morphology, domain sizes, surface functionalization, and dye

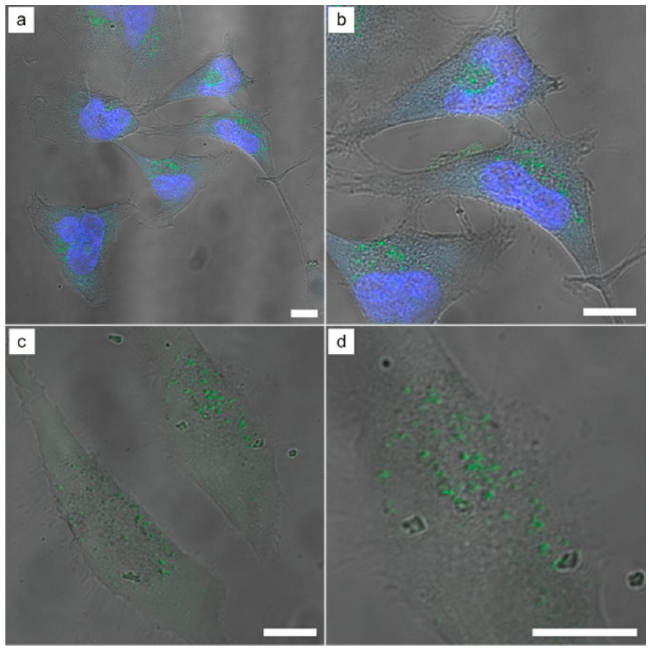

Figure 12. (a,b) Confocal laser scanning microscopy images of HeLa cells coincubated with Au@MnO@SiO_2–Atto495 (green) for 24 h at 37 °C. The cell nuclei (blue) were stained with DAPI. The sample was excited at 488 nm. (c,d) Two-photon images of the same sample, excited with a two-photon laser at 970 nm, 30 mW. Scale: 10 μm.

labeling. The metal oxide domain could be coated selectively with a thin silica layer, leaving the metal domain unaltered. The SiO_2 coating of the oxide domain provides water solubility and protection against ion leaching in a single step for converting the Janus nanoparticles into multifunctional, efficient vehicles for theranostics. The functionalized Au@ MnO@SiO_2 Janus particles were stable in water, buffer solution, and serum, showing no indication of aggregation.

The potential of the Au@MnO@SiO_2 Janus particles was explored by selective surface functionalization, taking advantage of the affinity of the individual components to different functional molecules. The functionalized nanoparticles are superparamagnetic and two-photon active, and they are therefore useful for simultaneous magnetic and optical detection. Time-resolved fluorescence spectroscopy in combination with CLSM revealed the silica-coated Au@MnO@SiO_2 heterodimers to be highly two-photon active, whereas no indication for an electronic interaction between the dye molecules incorporated in the silica shell surrounding the MnO domains and the attached Au domains was found. In addition, fluorescence quenching was observed when dye molecules were bound directly to the Au domains.

Cell viability assays carried out to judge the biocompatibility and potential biomedical applications revealed the Au@MnO@SiO_2 Janus particles to be non-cytotoxic. The versatility of Au@MnO@SiO_2 Janus particles may be extended to related multifunctional Janus nanoparticle systems for simultaneous optical, magnetic resonance (MRI), and computer tomography (CT) imaging.

■ ASSOCIATED CONTENT

Supporting Information

Details of the measurement and refinement of the X-ray diffraction data (Table S1); powder XRD pattern of Au@MnO-

particles (Figure S1); TEM-Tomography micrographs of Au@MnO heterodimers (Figure S2); UV−vis-spectra of Au@MnO and Au@MnO@SiO_2 nanoparticles with conjugated dyes (Figure S3); bleaching experiments of Texas Red-Au@MnO@SiO2-Atto495 using a 970 nm two-photon laser. (Figure S4); magnetic data of Au@MnO heterodimer-nanoparticles (Figure S5); two-photon fluorescence of Au@MnO@SiO_2 and Au@MnO@SiO_2−FITC nanoparticles (Figure S6); confocal image *z*-stacks showing the uptake of Au@MnO@SiO2 Janus-particles into HeLa cells (Figure S7). This material is available free of charge via the Internet at http://pubs.acs.org.

AUTHOR INFORMATION

Corresponding Author

tremel@uni-mainz.de

Notes

The authors declare no competing financial interest.

ACKNOWLEDGMENTS

This research was supported by the Deutsche Forschungsgesellschaft through the Priority Program 1313 "Bionanoresponses". F.L thanks the Max Planck Society for funding a Max Planck Research Group. I.S. acknowledges a "Fonds der Chemischen Industrie VCI"-Fellowship and is a recipient of a fellowship through the Excellence Initiative (DFG/GSC 266). D.G. is recipient of a Kekulé-Scholarship of the "Fonds der Chemischen Industrie". We are grateful to Dr. Thomas D. Schladt for his advice and input, and to Professor Manfred Schmidt for technical support regarding DLS measurements. The facilities of the Electron Microscopy Center in Mainz (EZMZ) were supported by the State Excellence Cluster COMATT and the SFB 625. Microscopy work of the LSM-Core Facility at the University Clinic in Mainz was supported by the Research Center for Immunology (FZI).

REFERENCES

(1) Wang, D.; Li, Y. *Adv. Mater.* **2011**, *23*, 1044−1060.
(2) Habas, S. E.; Lee, H.; Radmilovic, V.; Somorjai, G. A.; Yang, P. *Nat. Mater.* **2007**, *6*, 692−697.
(3) Joo, S. H.; Park, J. Y.; Tsung, C.-K.; Yamada, Y.; Yang, P.; Somorjai, G. A. *Nat. Mater.* **2009**, *8*, 126−131.
(4) Peng, Y.-K.; Lai, C.-W.; Liu, C.-L.; Chen, H.-C.; Hsiao, Y.-H.; Liu, W.-L.; Tang, K.-C.; Chi, Y.; Hsiao, J.-K.; Lim, K.-E.; Liao, H.-E.; Shyue, J.-J.; Chou, P.-T. *ACS Nano* **2011**, *5*, 4177−4187.
(5) Kim, T.; Momin, E.; Choi, J.; Yuan, K.; Zaidi, H.; Kim, J.; Park, M.; Lee, N.; McMahon, M. T.; Quinones-Hinojosa, A.; Bulte, J. W. M.; Hyeon, T.; Gilad, A. A. *J. Am. Chem. Soc.* **2011**, *133*, 2955−2961.
(6) Sun, S.; Murray, C. B.; Weller, D.; Folks, L.; Moser, A. *Science* **2000**, *287*, 1989−1992.
(7) Shevchenko, E. V.; Talapin, D. V.; Rogach, A. L.; Kornowski, A.; Haase, M.; Weller, H. *J. Am. Chem. Soc.* **2002**, *124*, 11480−11485.
(8) Alayoglu, S.; Eichhorn, B. *J. Am. Chem. Soc.* **2008**, *130*, 17479−17486.
(9) Liu, Z.; Hu, J. E.; Wang, Q.; Gaskell, K.; Frenkel, A. I.; Jackson, G. S.; Eichhorn, B. *J. Am. Chem. Soc.* **2009**, *131*, 6924−6925.
(10) Sinfeld, J. H. *Acc. Chem. Res.* **1987**, *20*, 134−139.
(11) Wetz, F.; Soulantica, K.; Falqui, A.; Respaud, M.; Snoeck, E.; Chaudret, B. *Angew. Chem., Int. Ed.* **2007**, *46*, 7079−7081.
(12) Sobal, N. S.; Hilgendorff, M.; Möhwaldt, H.; Spasova, M.; Radetic, T.; Farle, M. *Nano Lett.* **2002**, *2*, 621−624.
(13) Guo, S.; Dong, S.; Wang, E. *J. Phys. Chem. C* **2008**, *112*, 2389−2393.
(14) Lin, H. Y.; Chen, Y. F. *Appl. Phys. Lett.* **2006**, *88*, 161911.
(15) Perro, A.; Reculusa, S.; Ravaine, S.; Bourgeat-Lami, E.; Duguet, E. *J. Mater. Chem.* **2005**, *15*, 3745−3760.
(16) Vanakaras, A. G. *Langmuir* **2006**, *22*, 88−93.
(17) Ropponen, J.; Nummelin, S.; Rissanen, K. *Org. Lett.* **2004**, *6*, 2495−2497.
(18) Percec, V.; Imam, M. R.; Bera, T. K.; Balagurusamy, V. S. K.; Peterca, M.; Heiney, P. A. *Angew. Chem., Int. Ed.* **2005**, *44*, 4739−4745.
(19) Wang, J.; Liu, G.; Rivas, G. *Anal. Chem.* **2003**, *75*, 4667−4671.
(20) Erhardt, R.; Zhang, M. F.; Böker, A.; Zettl, H.; Abetz, C.; Frederik, P.; Krausch, G.; Abetz, V.; Müller, A. H. E. *J. Am. Chem. Soc.* **2003**, *125*, 3260−3267.
(21) Yu, H.; Chen, M.; Rice, P. M.; Wang, S. X.; White, R.; Sun, S. *Nano Lett.* **2005**, *5*, 379−382.
(22) Xu, C.; Xie, J.; Ho, D.; Wang, C.; Kohler, N.; Walsh, E.; Morgan, J.; Chin, Y.; Sun, S. *Angew. Chem., Int. Ed.* **2008**, *47*, 173−176.
(23) Xu, C.; Wang, B.; Sun, S. *J. Am. Chem. Soc.* **2009**, *131*, 4216−4217.
(24) Schladt, T. D.; Shukoor, M. I.; Tahir, M. N.; Natalio, F.; Schneider, K.; Ament, I.; Becker, J.; Jochum, F.; Weber, S.; Theato, P.; Schreiber, L. M.; Sönnichsen, C.; Schröder, H. C.; Müller, W. E. G.; Tremel, W. *Angew. Chem.* **2010**, *122*, 4068−4072; *Angew. Chem., Int. Ed.* **2010**, *49*, 3976−3980.
(25) Pacholski, C.; Kornowski, A.; Weller, H. *Angew. Chem.* **2004**, *116*, 4878−4881; *Angew. Chem., Int. Ed.* **2004**, *43*, 4774−4777.
(26) Fan, F.-R.; Ding, Y.; Liu, D.-Y.; Tian, Z.-Q.; Wang, Z. L. *J. Am. Chem. Soc.* **2009**, *131*, 12036−12037.
(27) Gu, H.; Yang, Z.; Gao, J.; Chang, C.; Xu, B. *J. Am. Chem. Soc.* **2005**, *127*, 34−35.
(28) Choi, S.-H.; Na, H. B.; Park, Y. I.; Kwangjin, A.; Kwon, S. G.; Jang, Y.; Park, M.-H.; Moon, J.; Son, J. S.; Song, C. I.; Moon, M. W.; Hyeon, T. *J. Am. Chem. Soc.* **2008**, *130*, 15573−15580.
(29) Hong, H.; Hu, L.; Li, M.; Zheng, J.; Sun, X.; Lu, X.; Cao, X.; Lu, J.; Gu, H. *Chem.—Eur. J.* **2011**, *17*, 8726−8730.
(30) Figuerola, A.; Fiore, A.; Di Corato, R.; Falqui, A.; Gianni, C.; Micotti, E.; Lascialfari, A.; Corti, M.; Cingolani, R.; Pellegrino, T.; Cozzoli, P. D.; Manna, L. *J. Am. Chem. Soc.* **2008**, *130*, 1477−1487.
(31) Schladt, T. D.; Graf, T.; Köhler, O.; Bauer, H.; Schneider, K.; Herold, C.; Mertins, J.; Tremel, W. *Chem. Mater.* **2012**, *24*, 525−535.
(32) Casavola, M.; Grillo, V.; Carlino, E.; Gozzo, F.; Pinel, E. F.; Garcia, M. A.; Manna, L.; Cingolani, R.; Cozzoli, P. D. *Nano Lett.* **2007**, *7*, 1386−1395.
(33) Nakhjavan, B.; Tahir, M. N.; Gao, H.; Schladt, T. D.; Schneider, K.; Natalio, F.; Ament, I.; Branscheid, R.; Weber, S.; Schröder, H.-C.; Müller, W. E. G.; Kolb, U.; Sönnichsen, C.; Schreiber, L. M.; Tremel, W. *J. Mater. Chem.* **2011**, *21*, 8605−8611.
(34) Nakhjavan, B.; Tahir, M. N.; Panthöfer, M.; Gao, H.; Gasi, T.; Ksenofontov, V.; Branscheid, R.; Weber, S.; Kolb, U.; Schreiber, L. M.; Tremel, W. *Chem. Commun.* **2011**, *47*, 8898−8900.
(35) Nakhjavan, B.; Tahir, M. N.; Natalio, F.; Panthöfer, M.; Gao, H.; Dietzsch, M.; Andre, R.; Gasi, T.; Ksenofontov, V.; Branscheid, R.; Kolb, U.; Tremel, W. *Nanoscale* **2012**, *4*, 4571−4577.
(36) Mokari, T.; Rothenberg, E.; Popov, I.; Costi, R.; Banin, U. *Science* **2004**, *304*, 1787−1790.
(37) Mokari, T.; Sztrum, C. G.; Salant, A.; Rabani, E.; Banin, U. *Nat. Mater.* **2005**, *4*, 855−863.
(38) Saunders, A. E.; Popov, I.; Banin, U. *J. Phys. Chem. B* **2006**, *110*, 25421−25429.
(39) Menagen, G.; Mocatta, D.; Salant, A.; Popov, I.; Dorfs, D.; Banin, U. *Chem. Mater.* **2008**, *20*, 6900−6902.
(40) Shi, W.; Zeng, H.; Sahoo, Y.; Ohulchanskyy, T. Y.; Ding, Y.; Wang, Z. L.; Swihart, M.; Prasad, P. N. *Nano Lett.* **2006**, *6*, 875−881.
(41) Yang, J.; Elim, H. I.; Zhang, Q.; Lee, J. Y.; Ji, W. *J. Am. Chem. Soc.* **2006**, *128*, 11921−11926.
(42) Yang, J.; Levina, L.; Sargent, E. H.; Kelley, S. O. *J. Mater. Chem.* **2006**, *16*, 4025−4028.
(43) Talapin, D. V.; Yu, H.; Shevchenko, E. V.; Lobo, A.; Murray, C. B. *J. Phys. Chem. C* **2007**, *111*, 14049−14054.
(44) Lee, J.-S.; Shevchenko, E. V.; Talapin, D. V. *J. Am. Chem. Soc.* **2008**, *130*, 9673−9675.
(45) Yang, J.; Ying, J. Y. *Chem. Commun.* **2009**, 3187−3189.

(46) Cayre, O.; Paunov, V. N.; Velev, O. D. *J. Mater. Chem.* **2003**, *13*, 2445−2450.
(47) Cayre, O.; Paunov, V. N.; Velev, O. D. *Chem. Commun.* **2003**, *8*, 2296−2297.
(48) Schladt, T. D.; Schneider, K.; Schild, H.-J.; Tremel, W. *Dalton Trans.* **2011**, *40*, 6315−6343.
(49) Yoon, D.; Lee, J.-H.; Shin, T.-H.; Cheon, J. *Acc. Chem. Res.* **2011**, *44*, 863−874.
(50) Kamaly, N.; Xiao, Z.; Valencia, P. M.; Radovic-Moreno, A. F.; Farokhzad, O. C. *Chem. Soc. Rev.* **2012**, *41*, 2971−3010.
(51) Teunissen, W.; Bol, A.; Geus, J. W. *Catal. Today* **1999**, *48*, 329−336.
(52) Shylesh, S.; Schünemann, V.; Thiel, W. R. *Angew. Chem., Int. Ed.* **2010**, *49*, 3428−3459.
(53) Kamat, P. V. *J. Phys. Chem. C* **2007**, *111*, 2834−2860.
(54) Costi, R.; Saunders, A. E.; Banin, U. *Angew. Chem., Int. Ed.* **2010**, *49*, 4878−4897.
(55) Du, J.; O'Reilly, R. K. *Chem. Soc. Rev.* **2011**, *40*, 2402−2416.
(56) Jain, P. K.; ElSayed, I. H.; El-Sayed, M. A. *Nano Today* **2007**, *2*, 18−29.
(57) Hvolbæk, B.; Janssens, T. V. W.; Clausen, B. S.; Falsig, H.; Christensen, C. H.; Nørskov, J. K. *Nano Today* **2007**, *2*, 14−18.
(58) Perez-Juste, J.; Pastoriza-Santos, I.; Liz-Marzan, L. M.; Mulvaney, P. *Coord. Chem. Rev.* **2005**, *249*, 1870−1901.
(59) Hu, M.; Chen, J.; Li, Z.-Y.; Au, L.; Hartland, G. V.; Li, X.; Marquez, M.; Xia, Y. *Chem. Soc. Rev.* **2006**, *35*, 1084−1094.
(60) Boyer, D.; Tamarat, P.; Maali, A.; Lounis, B.; Orrit, M. *Science* **2002**, *297*, 1160−1163.
(61) Sun, I.-C.; Eun, D.-K.; Na, J. H.; Lee, S.; Kim, I.-J.; Youn, I.-C.; Ko, C.-Y.; Kim, H.-S.; Lim, D.; Choi, K.; Messersmith, P. B.; Park, T. G.; Kim, S. Y.; Kwon, I. C.; Kim, K.; Ahn, C.-H. *Chem.—Eur. J.* **2009**, *15*, 13341−13347.
(62) Huang, X. H.; El-Sayed, I. H.; Qian, W.; El-Sayed, M. A. *J. Am. Chem. Soc.* **2006**, *128*, 2115−2120.
(63) Norman, R. S.; Stone, J. W.; Gole, A.; Murphy, C. J.; Sabo-Attwood, T. L. *Nano Lett.* **2008**, *8*, 302−306.
(64) Dickerson, E. B.; Dreaden, E. C.; Huang, X.; El-Sayed, I. H.; Chu, H.; Pushpanketh, S.; McDonald, J. F.; El-Sayed, M. A. *Cancer Lett.* **2008**, *269*, 57−66.
(65) Salgueirino-Maceira, V.; Correa-Duarte, M. A.; Farle, M. *Small* **2005**, *1*, 1073−1076.
(66) Durr, N. J.; Larson, T.; Smith, D. K.; Korgel, B. A.; Sokolov, K.; Ben-Yakar, A. *Nano Lett.* **2007**, *7*, 941.
(67) Wang, H. F.; Huff, T. B.; Zweifel, D. A.; He, W.; Low, P. S.; Wei, A.; Cheng, J. X. *Proc. Natl. Acad. Sci. U.S.A.* **2005**, *102*, 15752.
(68) Sevick-Muraca, E. M.; Houston, J. P.; Gurfinkel, M. *Curr. Opin. Chem. Biol.* **2002**, *6*, 642−650.
(69) Larson, D. R.; Zipfel, W. R.; Williams, R. M.; Clark, S. W.; Bruchez, M. P.; Wise, F. W.; Webb, W. W. *Science* **2003**, *300*, 1434−1438.
(70) Tsoi, K. M.; Dai, Q.; Alman, B. A.; Chan, W. C. *Acc. Chem. Res.* **2013**, *46*, 662−671.
(71) Wang, D.-S.; Hsu, F.-Y.; Lin, C.-W. *Opt. Express* **2009**, *17*, 11350−11359.
(72) Cao, L.; Wang, X.; Meziani, M. J.; Lu, F.; Wang, H.; Luo, P. G.; Lin, Y.; Harruff, B. A.; Veca, L. M.; Murray, D.; Xie, S.-Y.; Sun, Y.-P. *J. Am. Chem. Soc.* **2007**, *129*, 11318−11319.
(73) Tu, C.; Ma, X.; Pantazis, P.; Kauzlarich, S. M.; Louie, A. Y. *J. Am. Chem. Soc.* **2010**, *132*, 2016−2023.
(74) Hilderbrand, S. A.; Shao, F.; Salthouse, C.; Mahmood, U.; Weissleder, R. *Chem. Commun.* **2009**, 4188−4190.
(75) Jun, C. H.; Park, Y. J.; Yeon, Y. R.; Choi, J. R.; Lee, W. R.; Ko, S. J.; Cheon, J. *Chem. Commun.* **2006**, 1619−1621.
(76) Kang, S. S.; Miao, G. X.; Shi, S.; Jia, Z.; Nikles, D. E.; Harrell, J. W. *J. Am. Chem. Soc.* **2006**, *128*, 1042−1043.
(77) Jun, Y. W.; Seo, J.-W.; Cheon, J. W. *Acc. Chem. Res.* **2008**, *41*, 179−189.
(78) Bodnarchuk, M. I.; Kovalenko, M. V.; Groiss, H.; Resel, R.; Reissner, M.; Hesser, G.; Lechner, R. T.; Steiner, W.; Schäffler, F.; Heiss, W. *Small* **2009**, *5*, 2247−2252.
(79) Schröder, H. C.; Natalio, F.; Shukoor, M. I.; Tahir, M. N.; Tremel, W.; Belikov, S. I.; Krasko, A.; Müller, W. E.G. *Mol. Immunol.* **2008**, *45*, 945−953.
(80) Shukoor, M. I.; Natalio, F.; Krasko, A.; Schröder, H. C.; Müller, W. E. G.; Tremel, W. *Chem. Commun.* **2007**, 4677−4679.
(81) Reineke, J. *Pharmaceutical Sciences Encyclopedia: Drug Discovery, Development, and Manufacturing* **2010**, 1−21.
(82) Beveridge, J. S.; Stephens, J. R.; Williams, M. E. *Annu. Rev. Anal. Chem.* **2011**, *4*, 251−273.
(83) Sun, C.; Lee, J. S. H.; Zhang, M. *Adv. Drug Delivery Rev.* **2008**, *60*, 1252−1265.
(84) Lacroix, L. M.; Ho, D.; Sun, S. *Curr. Top. Chem.* **2010**, *10*, 1184−1197.
(85) Kim, J.; Park, S.; Lee, J. E.; Jin, S. M.; Lee, J. H.; Lee, I. S.; Yang, I.; Kim, J. S.; Kim, S. K.; Cho, M. H.; Hyeon, T. *Angew. Chem.* **2006**, *118*, 7918−7922; *Angew. Chem., Int. Ed.* **2006**, *45*, 7754−7758.
(86) Liong, M.; Lu, J.; Kovochich, M.; Xia, T.; Ruehum, S. G.; Nel, A. E.; Tamanoi, F.; Zink, J. I. *ACS Nano* **2008**, *2*, 889−896.
(87) Wang, L. Y.; Bai, J. W.; Li, Y. J.; Huang, Y. *Angew. Chem.* **2008**, *120*, 2473−2476; *Angew. Chem., Int. Ed.* **2008**, *47*, 2439−2443.
(88) Park, H.; Yang, J.; Seo, S.; Kim, K.; Suh, J.; Kim, D.; Haam, S.; Yoo, K. H. *Small* **2008**, *4*, 192−196.
(89) Kim, C.-K.; Ghosh, P.; Rotello, V. M. *Nanoscale* **2009**, *1*, 61−67.
(90) Mansson, S., Bjornerud, A. In *The Chemistry of Contrast Agents in Medical Magnetic Resonance Imaging*; Merbach, A. E., Toth, E., Eds.; Wiley: New York, 2001; pp 1−44.
(91) Jun, Y. W.; Lee, J. H.; Cheon, J. W. *Angew. Chem.* **2008**, *120*, 5200−5213; *Angew. Chem., Int. Ed.* **2008**, *47*, 5122−5135.
(92) Na, H. B.; Lee, J. H.; An, K.; Park, Y. I.; Park, M.; Lee, I. S.; Nam, D. H.; Kim, S. T.; Kim, S. H.; Kim, S. W.; Lim, K. H.; Kim, K. S.; Kim, S.-O.; Hyeon, T. *Angew. Chem.* **2007**, *119*, 5493−5497; *Angew. Chem., Int. Ed.* **2007**, *46*, 5397−5401.
(93) Kai, W.; Xiaojun, X.; Ximing, P.; Zhenqing, H.; Oiqing, Z. *Nanoscale Res. Lett.* **2011**, *6*, 480.
(94) Shukoor, M. I.; Natalio, F.; Gupta, P.; Wiens, M.; Tarantola, M.; Barz, M.; Weber, S.; Terekhov, M.; Schröder, H. C.; Müller, W. E. G.; Janshoff, A.; Theato, P.; Zentel, R.; Schreiber, L. M.; Tremel, W. *Adv. Funct. Mater.* **2009**, *9*, 3717−3725.
(95) Choi, J. Y.; Lee, S. H.; Na, H. B.; An, K.; Hyeon, T.; Seo, T. S. *Bioprocess Biosyst. Eng.* **2010**, *33*, 21−30.
(96) Schladt, T. D.; Koll, K.; Prüfer, S.; Bauer, H.; Natalio, F.; Dumele, O.; Raidoo, R.; Weber, S.; Wolfrum, U.; Schreiber, L. M.; Radsak, M. P.; Schild, H.; Tremel, W. *J. Mater. Chem.* **2011**, *22*, 9253−9262.
(97) Sotirou, G. A.; Hirt, A. M.; Lozach, P.-Y.; Teleki, A.; Krumeich, F.; Pratsinis, S. E. *Chem. Mater.* **2011**, *23*, 1985−1992.
(98) Peng, S.; Lee, Y.; Wang, C.; Yin, H.; Dai, S.; Sun, S. *Nano Res* **2008**, *1*, 229−234.
(99) Schladt, T. D.; Graf, T.; Tremel, W. *Chem. Mater.* **2009**, *21*, 3183−3190.
(100) Wang, C.; Xu, C.; Zeng, H.; Sun, S. *Adv. Mater.* **2009**, *21*, 3045−305.
(101) Mie, G. *Ann. Phys.* **1908**, *330*, 377−445.
(102) Daniel, M.-C.; Astruc, D. *Chem. Rev* **2004**, *104*, 293−346.
(103) Kelly, K. L.; Coronado, E.; Zhao, L. L.; Schatz, G. C. *J. Phys. Chem. B* **2003**, *107*, 668−677.
(104) Storhoff, J. J.; Elghanian, R.; Mucic, R. C.; Mirkin, C. A.; Letsinger, R. L. *J. Am. Chem. Soc.* **1998**, *120*, 1959−1964.
(105) Beutler, B.; Eidenschenk, C.; Crozat, K.; Imler, J.-L.; Takeuchi, O.; Hoffmann, J. A.; Akira, S. *Nat. Rev. Immunol.* **2007**, *7*, 753−766.
(106) Shukoor, M. I.; Natalio, F.; Glube, N.; Tahir, M. N.; Therese, H. A.; Ksenofontov, V.; Metz, N.; Theato, P.; Langguth, P.; Boissel, J.-P.; Schröder, H.-C.; Müller, W. E. G.; Tremel, W. *Angew. Chem.* **2008**, *120*, 4826−4830; *Angew. Chem., Int. Ed.* **2008**, *47*, 4748−4752.
(107) Shukoor, M. I.; Natalio, F.; Schladt, T. D.; Koll, K.; Tahir, M. N.; Barz, M.; Weber, S.; Brochhausen, C.; Zentel, R.; Wiens, M.;

Schreiber, L. M.; Brieger, J.; Müller, W. E. G.; Tremel, W. *J. Mater. Chem.* **2011**, *22*, 8826−8834.